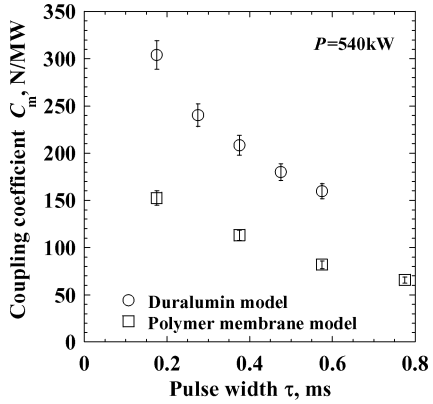

Fig. 7 Momentum-coupling coefficient.

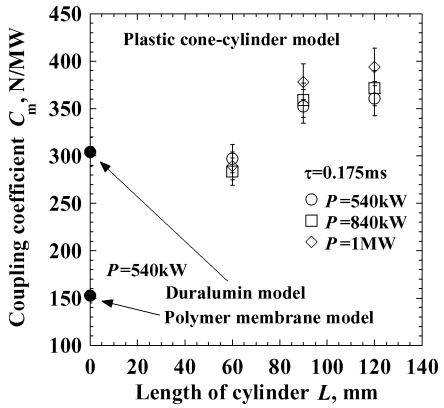

Fig. 8 Momentum-coupling coefficient and vehicle length.

duralumin model. This would be because the polymer membrane parabola was less rigid than the duralumin one, and shock reflection on the membrane became inelastic.

For both models C_m decreased with τ. This would be because, in the long pulse case, most of the energy was provided to the plasma developed outside of the parabola, and the pressure of the plasma was not converted to the thrust. Optimum pulse width for this scale of parabola would be shorter than 0.175 ms.

Figure 8 shows measured C_m for the cone–cylinder model along with those for the parabola models. It was deduced from v_0. C_m increased monotonically with the length of cylinder L. This indicates that the pressure of plasma was effectively converted to thrust by the cylinder portion of the model. The effect of rigidity of the cone–cylinder model would be similar to that of the membrane model.

Maximum C_m of 395 N/MW was recorded at $\tau = 0.175$ ms, $P = 1$ MW, and $L = 120$ mm. This value was comparable to those of laser-boosted vehicles.[7–9]

Conclusions

Using a 1-MW gyrotron, microwave-boosted vehicle models were launched, and propulsive impulse was measured by three methods. Results showed good agreement among measurement methods.

We estimated the momentum-coupling coefficient from the measured propulsive impulse. As a result, the maximum coupling coefficient of 395 N/MW was obtained with the cone–cylinder model. This value was comparable to those of laser-boosted vehicles.

The coupling coefficient will be increased further by optimizing pulse width and vehicle length as well as by increasing rigidity of the vehicle structure.

References

[1]Myrabo, L. N., "Ground and Flight Tests of a Laser Boosted Vehicle," AIAA Paper 98-1001, 1998.

[2]Schall, W. O., Bohn, W. L., Eckel, H.-A., Mayerhofer, W., Riede, W., and Zeyfang, E., "Lightcraft Experiments in Germany," *Proceedings of the SPIE: High-Power Laser Ablation III*, Vol. 4065, edited by C. R. Phipps, International Society for Optical Engineering, Bellingham, WA, 2000, pp. 472–481.

[3]Katsurayama, H., Komurasaki, K., and Momozawà, A., and Arakawa, Y., "Numerical and Engine Cycle Analyses of a Pulsed Laser Ramjet Vehicle," *Space Technology Japan*, Vol. 1, Sept. 2003, pp. 9–16.

[4]Benford, J., and Dickinson, R., "Space Propulsion and Power Beaming Using Millimeter Systems," *Proceedings of the SPIE: Intense Microwave Pulses III*, Vol. 2557, edited by H. E. Brandt, Society of Photo-Optical Instrumentation Engineers, Bellingham, WA, 1995, pp. 179–192.

[5]Sahara, H., "Ultra-Light Electromagnetic Wave Concentrator with Variable Focal Length and Its Use for Solar Thermal Propulsion," International Symposium on Space Technology and Science, 2002-c-19, Tokyo, May–June 2002.

[6]Sakamoto, K., Kasugai, A., Tsuneoka, M., Takahashi, K., Imai, T., Kariya, T., and Mitsunaka, Y., "High Power 170 GHz Gyrotron with Synthetic Diamond Window," *Review of Scientific Instruments*, Vol. 70, No. 1, 1999, pp. 208–212.

[7]Myrabo, L. N., Libeau, M. A., Meloney, E. D., Bracken, R. L., and Knowles, T. B., "Pulsed Laser Propulsion Performance of 11-cm Parabolic 'Bell' Engines Within the Atmosphere," AIAA Paper 2002-2204, 2002.

[8]Bohn, W. L., "Laser Lightcraft Performance," *Proceedings of the SPIE: High-Power Laser Ablation II*, Vol. 3885, edited by C. R. Phipps and M. Niino, International Society for Optical Engineering, Bellingham, WA, 2000, pp. 48–53.

[9]Mori, K., Katsurayama, H., Hirooka, Y., Komurasaki, K., and Arakawa, Y., "An Experimental Study on the Energy Balance in the Repetitively Pulsed Laser Propulsion," AIAA Paper 2003-496, 2003.

I. Boyd
Associate Editor

Optimal Ascent Trajectory for Efficient Air Launch into Orbit

Frederick W. Boltz*
Launch Vehicle Technology, Sunnyvale, California 94087

Introduction

SINCE early in 2001, various teams of contractors have been funded for the Responsive Small Cargo Affordable Launch (RASCAL) project.[1] The stated goal of the RASCAL project is development of a low-cost, small-satellite launcher with the capability of delivering a 50–75-kg payload to low Earth orbit (LEO). The initial concept being pursued is that of miniature rocket launch from an airbreathing carrier aircraft at high altitude to provide independence from use of a dedicated launch facility (with a significant saving in ground-support costs). The critical part of the concept is the feasibility of developing a new type of carrier aircraft with a "souped-up" turbojet engine as a reusable booster stage. Air launch of the rocket would occur at about 130,000 ft (39.6 km) with the rocket continuing its ascent to orbit and the carrier aircraft descending for a runway landing. It is anticipated that the gross takeoff weight of an aircraft and a 6000-lb rocket would be about 22,000 lb.

There has been only one air-launch system developed among all the U.S. space launch vehicles. The Pegasus XL[2] is a three-stage, solid-propellant rocket that is air launched horizontally from an L-1011 TriStar aircraft for LEO. The rocket has a delta wing attached

Received 11 April 2003; revision received 10 September 2003; accepted for publication 10 September 2003.

*Aerospace Engineer; currently Senior Consultant, Knowledge Systems Design, Inc., Newport Beach, CA 92663. Senior Member AIAA.

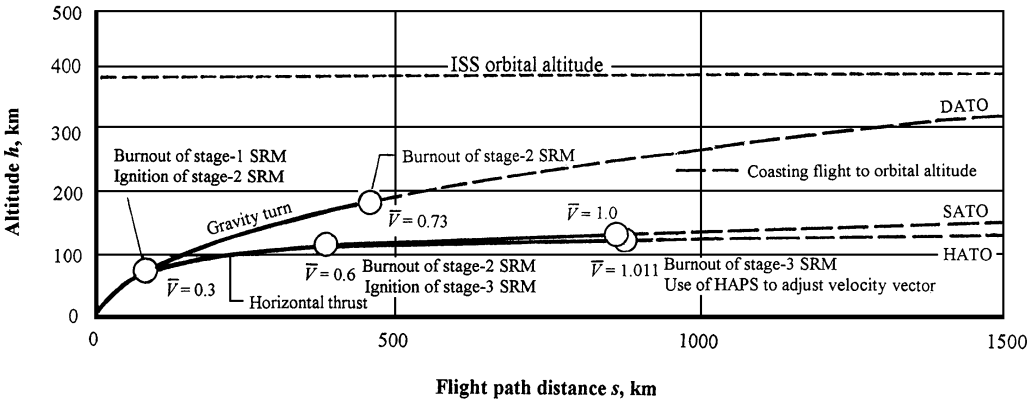

Fig. 1 Comparison of ascent flight path for DATO with that for SATO and HATO.

to the first stage (for turning the flight path upward through the lower atmosphere) and weighs about 51,000 lb (including a 977-lb payload for the lowest LEO). As with all solid-propellant rockets, the accuracy of placing the payload into a precise orbit has been limited by an inability to vary the duration of final-stage thrusting. This limitation has been removed in a later version of the Pegasus XL by addition of a small hydrazine auxiliary propulsion system (HAPS) to the final stage (inside the avionics deck behind the payload). This monopropellant thruster permits vernier adjustments to orbital velocity after burnout of the third-stage solid rocket motor (SRM). A half-size version of this HAPS add-on could also be useful with miniature rockets of the size required to place small satellites in orbit. If all dimensions of the Pegasus XL were halved, it would weigh 1/8th as much (or 6375 lb) with the capability of placing a 122-lb payload in the lowest LEO.[3]

In a previous Note[3] an alternative low-cost system (to that being studied in the RASCAL project) was proposed for air launch of miniature rockets into orbit using existing jet trainers/fighters as relatively inexpensive carrier aircraft. It was shown that specific launch costs (i.e., costs per pound of payload) for this type of system would probably be less than such costs for the RASCAL system or any ground-launched rocket. The purpose of this Note is to determine an optimal ascent trajectory for maximizing the payload capability of a miniature rocket air launched into the 240-mile orbit of the International Space Station (ISS). Three different types of ascent trajectory are considered in the study to find an optimal flight path to follow after leaving the sensible atmosphere. The three types of flight path consist of 1) conventional direct ascent to orbit (DATO), 2) shuttle-like ascent to orbit (SATO), and 3) Hohmann-like ascent to orbit (HATO). The latter two are similar in that orbital speed is attained at an altitude just above the sensible atmosphere. However, most launches (both air and ground) utilize direct ascent to orbit for a variety of reasons. Perhaps the most compelling reason is that of getting into orbit quickly. If there is no time constraint, the greater payload advantage of a Shuttle-like ascent should probably be considered in the planning of any launch into orbit. The Hohmann type of ascent is regularly used in transferring spacecraft from one near-circular orbit to another higher near-circular orbit.[4] A HAPS add-on to the avionics and payload module of a miniature rocket would be required for both shuttle and Hohmann types of ascent. Although not required for direct ascent, a HAPS add-on would enable precise final correction of the orbit.

General Considerations

In the analysis of payload capability, it has been assumed that the miniature air-launched rockets are similar to half-size versions of the Pegasus XL with solid rocket motors in the three stages and a half-size HAPS attached to the avionics and payload module. However, the delta wing on the first stage has been deleted with a saving in weight but a necessity of air launch at high flight-path angle. Because the effects of aerodynamic drag are relatively minor in comparison to other effects, they have been ignored in the analysis. As is shown in Fig. 1, the three types of flight path considered share a common gravity turn following air launch and separation of the rocket first stage (after burnout of its SRM). In the conventional DATO case the rocket continues along a gravity turn following ignition of the second-stage SRM. Coasting flight to near orbital altitude occurs after burnout of the second-stage SRM and separation of the second stage. Final acceleration to orbital speed begins near orbital altitude with ignition of the third-stage SRM. After burnout of the third-stage SRM and separation of the third stage, vernier adjustment of the velocity vector (speed and/or direction) of the payload module can be made using the HAPS unit.

The second type of ascent flight path considered is similar to that used in a typical shuttle launch, where acceleration to orbital speed occurs during a shallow dive and slight climb just above the sensible atmosphere (and after earlier separation of the burned-out solid rocket boosters in the lower atmosphere). A long period of coasting flight and separation of the external tank is followed by circularization of the orbit near apogee. In the case of an air-launched miniature rocket using the SATO flight path, a gravity turn results from first-stage thrusting at zero thrust angle. Following burnout of the first-stage SRM and separation of the rocket first stage, the vehicle is pitched down to a horizontal attitude prior to ignition of the second-stage SRM. Then, with thrust in a horizontal direction (and upward momentum to climb out of the sensible atmosphere) a flattening of the flight path occurs during acceleration to higher speed. After burnout of the second-stage SRM and separation of the second stage, ignition of the third-stage SRM (with thrust slightly inclined to the horizontal) allows acceleration to continue along a nearly horizontal flight path just above the sensible atmosphere. Ideally, burnout of the third-stage SRM occurs when orbital speed is attained and the flight-path angle has the precise required value. In any case, the HAPS unit can be used to rotate the velocity vector the necessary amount and adjust its magnitude (speed). Then, after a long period of coasting flight, final circularization of the orbit occurs at apogee using the HAPS unit again.

The third type of ascent flight path considered is that normally associated with the most-efficient Hohmann transfer from one circular orbit to another coplanar circular orbit along an ellipse, which is tangent to the two circular orbits. In the case of an air-launched miniature rocket the sequence of events in a HATO flight path is nearly the same as that for the second type of ascent flight path (SATO). The difference is that during third-stage acceleration to orbital speed just above the sensible atmosphere the thrust direction is kept horizontal as the flight-path angle approaches 0. Then, after separation of the third stage the HAPS unit is used to slightly increase the orbital speed while maintaining zero flight-path angle. Moreover, the period of coasting flight following final SRM burnout and first use of the HAPS is nearly twice as long. But the total amount of HAPS monopropellant ideally required for speed increase and for orbit circularization at apogee is about the same as for SATO.

Table 1 Nominal flight conditions along a direct ascent trajectory during air launch of a miniature rocket into ISS orbit[a]

h, km	$\bar{V}$	γ, deg	τ, deg	r, km	s, km	$\sqrt{(r/g)}$, s	t, s	V, km/s	m/m_0
391.4	1.0	0.0	0	6769	2292	880.0	540.0	7.692	0.01832
Vernier correction of velocity vector using HAPS									0.01832
Separation of stage 3 after burnout of SRM									−0.00363[b]
391.4	1.0	0.0	0	6769	2292	880.0	533.2	7.692	0.02195
391.2	0.9	0.15	0	6769	2137	879.9	510.8	6.924	0.02973
390.3	0.8	0.62	0	6768	2001	879.8	488.7	6.154	0.04028
388.1	0.7	1.46	0	6766	1881	879.3	466.5	5.387	0.05462
Ignition of stage-3 SRM									
Coasting flight: $e = 0.51047$, $r_2/r_1 = 1.03005$									0.05462
Separation of stage 2 after burnout of SRM									−0.02443[b]
190.7	0.73	13.6	0	6569	462	842.5	196.3	5.692	0.07905
179.2	0.7	14.0	0	6557	418	840.5	187.4	5.461	0.08723
157.9	0.6	15.0	0	6536	326	836.5	170.4	4.688	0.11781
130.0	0.5	17.0	0	6508	240	831.2	146.6	3.915	0.16007
101.4	0.4	20.0	0	6479	155	825.8	120.7	3.138	0.21842
76.0	0.3	24.0	0	6454	93	819.6	95.9	2.363	0.29889
Separation of stage 1 after burnout of SRM, ignition of stage-2 SRM									−0.07011[b]
76.0	0.3	24.0	0	6454	93	819.6	95.9	2.363	0.36900
53.1	0.2	30.0	0	6431	48	815.3	70.2	1.578	0.50868
23.1	0.1	45.0	0	6401	10	810.2	28.8	0.790	0.74361
11.0	0.03	63.0	0	6389	0	807.9	0	0.237	1.00000
Ascent by carrier aircraft									

[a]Time parameter $\sqrt{(r/g)} = 805.8 + 0.19\,h$ in s. Circular orbital speed $\sqrt{gr} = r/\sqrt{(r/g)}$ in km/s. Velocity $V = \sqrt{(gr)}\bar{V}$ in km/s.
[b]Stage inert weight fraction.

Table 2 Nominal flight conditions along a shuttle-type ascent trajectory during air launch of a miniature rocket into ISS orbit[a]

h, km	$\bar{V}$	γ, deg	τ, deg	r, km	s, km	$\sqrt{(r/g)}$, s	t, s	V, km/s	m/m_0
391.4	1.0	0.0	0	6769	10,708	880.0	1,650.0	7.692	0.02150
Circularization of orbit using HAPS									0.02150
391.4	0.98	0.0	0	6769	10,708	880.0	1,638.0	7.538	0.02314
Coasting flight, $e = 0.04048$, $r_2/r_1 = 1.04048$									0.02314
Vernier correction of velocity vector using HAPS									0.02314
Separation of stage 3 after burnout of SRM									−0.00731[b]
134.0	1.0	2.32	2.4	6512	858	831.3	254.5	7.834	0.03045
108.0	0.6	4.0	2.4	6486	384	826.3	179.0	4.710	0.09627
Separation of stage 2 after burnout of SRM, ignition of stage-3 SRM									−0.02026[b]
108.0	0.6	4.0	−4	6486	384	826.3	179.0	4.710	0.11653
76.0	0.3	24.0	−24	6454	93	819.6	95.9	2.362	0.29889
Separation of stage 1 after burnout of SRM, ignition of stage-2 SRM									−0.07011[b]
76.0	0.3	24.0	0	6454	93	819.6	95.9	2.363	0.36900
53.1	0.2	30.0	0	6431	48	815.3	70.2	1.578	0.50868
23.1	0.1	45.0	0	6401	10	810.2	28.8	0.790	0.74361
11.0	0.03	63.0	0	6389	0	807.9	0	0.237	1.00000
Ascent by carrier aircraft									

[a]Time parameter $\sqrt{(r/g)} = 805.8 + 0.19\,h$ in s. Circular orbital speed $\sqrt{gr} = r/\sqrt{(r/g)}$ in km/s. Velocity $V = \sqrt{(gr)}\bar{V}$ in km/s.
[b]Stage inert weight fraction.

Results and Discussion

The miniature rocket motion and mass loss along each of the three ascent flight paths considered were computed using approximate stepwise solutions of the equations of motion and the generalized rocket equation (which accounts for changes in altitude, velocity, flight-path angle, and thrust angle). Nominal flight conditions for air launch of a miniature 7000-lb rocket into ISS orbit are listed in Tables 1, 2, and 3 for DATO, SATO, and HATO, respectively. From these results were obtained the estimated weights of various rocket components and the required average thrust levels of each-stage SRM presented in Table 4. It was assumed that the inert weight of each stage would be 10% of the total stage weight so that the amount of solid propellant and any expendable gas for attitude control would comprise 90% of the total stage weight.

Nominal flight conditions for the three types of rocket ascent to orbit considered after air launch are the same until burnout of the SRM in the first stage and separation of that stage. For DATO the rocket continues along a gravity-turn trajectory after ignition of the second-stage SRM. For both SATO and HATO the rocket is first pitched down to a horizontal attitude prior to ignition of the second-stage SRM. The upward momentum generated by first-stage thrusting keeps the rocket climbing along a steadily flattening flight path as gravity causes a deceleration of the vertical component of velocity and horizontal thrusting causes an acceleration of the velocity vector. The purpose of using horizontal thrust is to keep the altitude from increasing too much while efficient use of thrust is made during acceleration to orbital speed. This is not quite the same as in the case of a typical shuttle launch into orbit, where the thrust angle is greater during final acceleration to orbital speed.[5,6]

In Tables 2 and 3 it is seen that flight conditions are identical for SATO and HATO until separation of the second stage. For SATO the thrust angle is inclined slightly upward from the horizontal during stage-3 thrusting so that the flight-path angle decreases from 4 deg to only about 2.32 deg at SRM burnout (and, ideally, $\bar{V} = 1$). The result is coasting flight along an ellipse of higher eccentricity (0.04048). For HATO thrusting is maintained in the horizontal direction during stage-3 thrusting, and, after SRM burnout and separation of that stage, the HAPS unit is used to slightly lengthen the velocity vector.

Table 3 Nominal flight conditions along a Hohmann-type ascent trajectory during air launch of a miniature rocket into ISS orbit[a]

h, km	$\bar{V}$	γ, deg	τ, deg	r, km	s, km	$\sqrt{(r/g)}$, s	t, s	V, km/s	m/m_0
391.4	1.0	0.0	0	6769	20,573	880.0	2,950.0	7.692	0.02150
Circularization of orbit using HAPS									0.02150
391.4	0.989	0.0	0	6769	20,573	880.0	2,945.5	7.607	0.02234
Coasting flight, $e = 0.01984$, $r_2/r_1 = 1.04048$									0.02234
125.0	1.011	0.0	0	*Increase in orbital speed using HAPS*				7.925	0.02234
Separation of stage 3 after burnout of SRM									−0.00731[b]
125.0	1.0	0.0	0	6503	873	829.6	256.9	7.839	0.03045
108.0	0.6	4.0	−4	6486	384	826.3	179.0	4.710	0.09627
Separation of stage 2 after burnout of SRM, ignition of stage-3 SRM									−0.02026[b]
108.0	0.6	4.0	−4	6486	384	826.3	179.0	4.710	0.11653
76.0	0.3	24.0	−24	6454	93	819.6	95.9	2.362	0.29889
Separation of stage 1 after burnout of SRM, ignition of stage-2 SRM									−0.07011[b]
76.0	0.3	24.0	0	6454	93	819.6	95.9	2.363	0.36900
53.1	0.2	30.0	0	6431	48	815.3	70.2	1.578	0.50868
23.1	0.1	45.0	0	6401	10	810.2	28.8	0.790	0.74361
11.0	0.03	63.0	0	6389	0	807.9	0	0.237	1.00000
Ascent by carrier aircraft									

[a]Time parameter $\sqrt{(r/g)} = 805.8 + 0.19\,h$ in s. Circular orbital speed $\sqrt{gr} = r/\sqrt{(r/g)}$ in km/s. Velocity $V = \sqrt{(gr)}\bar{V}$ in km/s.
[b]Stage inert weight fraction.

Table 4 Estimated component specifications of miniature rockets weighing 7000 lb when air launched along three different flight paths into ISS orbit

	Type of ascent trajectory		
Component	DATO	SATO	HATO
Stage 1			
Inert weight, lb(kg)	491(224)	491(224)	491(224)
Propellant weight, lb(kg)	4,417(2,008)	4,417(2,008)	4,417(2,008)
Total weight, lb(kg)	4,908(2,231)	4,908(2,231)	4,908(2,231)
Specific impulse I_{sp}, s	280	280	280
Average thrust, lb(N)	12,900(57,400)	12,900(57,400)	12,900(57,400)
Thrust duration, s	96	96	96
Stage 2			
Inert weight, lb(kg)	171(78)	142(65)	142(65)
Propellant weight, lb(kg)	1,539(700)	1,276(580)	1,276(580)
Total weight, lb(kg)	1,710(777)	1,418(645)	1,418(645)
Specific impulse, I_{sp}, s	290	290	290
Average thrust, lb(N)	4,445(19,780)	4,450(19,800)	4,450(19,800)
Thrust duration, s	100	83	83
Stage 3			
Inert weight, lb(kg)	25(11)	51(24)	51(24)
Propellant weight, lb(kg)	229(104)	461(210)	460(209)
Total weight, lb(kg)	254(115)	513 (233)	512(233)
Specific impulse I_{sp}, s	290	290	290
Average thrust, lb(N)	1,000(4,450)	1,435(6,400)	1,025(4,565)
Thrust duration, s	67	93	130
Payload module			
Inert weight, lb(kg)	35(16)	35(16)	35(16)
Avionics weight, lb(kg)	25(11)	25(11)	25(11)
Hydrazine weight, lb(kg)[a]	10(5)	22(10)	22(10)
Specific impulse I_{sp}, s	230	230	230
Payload weight, lb(kg)	58(26)	79(36)	80(36)
Total weight, lb(kg)	128(58)	161(73)	162(74)
Weight in ISS orbit, lb (kg)	128(58)	149(68)	150(68)

[a]Includes an extra 10 lb for contingency thrusting.

The result is coasting flight along an ellipse of lower eccentricity (0.01984). At apogee a lessor amount of HAPS propellant is required for HATO than for SATO to circularize the orbit, but the total amount of hydrazine propellant used is about the same. The overall effect is that the total weight delivered to ISS orbit is about 16% more for either SATO or HATO than for DATO. A comparison of estimated component weights and average thrust levels of the SRMs in the three stages is shown in Table 4. The estimated inert weight of the payload module and weight of avionics required might not be truly representative of existing technology. However, it is indicated that a minimum increase of about 20 lb in payload capability can be achieved by using either SATO or HATO rather than DATO after air launch of a miniature rocket.

Conclusions

An optimal ascent trajectory for maximizing the payload capability of a miniature rocket air launched into orbit is nominally one that results in orbital speed being attained at an altitude just above the sensible atmosphere. This type of ascent trajectory is used in typical shuttle launches of heavy payloads into orbit. However, in a typical shuttle launch there are necessarily some steering losses that can be avoided when the launch vehicle is considerably smaller with a lower drag coefficient. The way to minimize steering (and gravity) losses after a gravity turn is to pitch the miniature rocket down to a horizontal attitude (with negative thrust angle) prior to leaving the sensible atmosphere. This results in a flattening of the

flight path along with most efficient use of thrust to accelerate the rocket to orbital speed at the lowest possible altitude. In the case of the shuttle, the thrust angle has to be positive (but generally decreasing) during final acceleration to orbital speed (which results in the larger steering losses). The Hohmann type of ascent is slightly more efficient than the shuttle type of ascent (in getting the greatest weight into orbit), but it takes nearly twice as long. In turn, the shuttle type of ascent takes considerably longer than direct ascent. The primary advantage of Hohmann ascent or shuttle ascent over direct ascent is that the same weight rocket can deliver about 16% more total weight to the 240-mile orbit of the International Space Station (ISS). For subsonic air launch (at about 40,000-ft altitude and high flight-path angle) of a miniature rocket weighing 7000 lb, the total weight delivered to the ISS orbit increases from about 128 lb to about 150 lb in changing from direct ascent to either shuttle or Hohmann ascent. It is conjectured that the disparity in total weight placed in orbit should increase with an increase in orbital altitude.

References

[1]Wall, R., "New Launcher Eyed for Small Satellites," *Aviation Week and Space Technology*, Vol. 155, No. 19, 2001, pp. 64, 65.

[2]Isakowitz, S. J., Hopkins, J. P., Jr., and Hopkins, J. B., *International Reference Guide to Space Launch Systems*, 3rd ed., AIAA, Reston, VA, 1999, pp. 267–279.

[3]Boltz, F. W., "Low-Cost Small-Satellite Delivery System," *Journal of Spacecraft and Rockets*, Vol. 39, No. 5, 2002, pp. 818–820.

[4]Humble, R. W., Henry, G. N., and Larson, W. J. (eds.), *Space Propulsion Analysis and Design*, McGraw–Hill, New York, 1995, pp. 47–52.

[5]Boltz, F. W., "Analytic Solution for Vertical Launch into Orbit," *Journal of the Astronautical Sciences*, Vol. 37, No. 4, 1989, pp. 491–511.

[6]Logsdon, T., *Orbital Mechanics, Theory and Application*, Wiley, New York, 1998, p. 155.

J. Martin
Associate Editor

Oblate Earth Eclipse State Algorithm for Low-Earth-Orbiting Satellites

Sima Adhya,* Anthony Sibthorpe,† Marek Ziebart,‡ and Paul Cross§
University College London, London, England WC1E 6BT, United Kingdom

Introduction

EARTH-ORBITING satellites experience partial or total eclipses when they pass through the regions known as the umbra and penumbra. In the penumbra, the total solar irradiance is partially occluded by the Earth, whereas the umbra can be defined as the region on the antisun side of the Earth, which is completely devoid of solar radiation.

Figure 1 shows the umbra and penumbra regions for a spherical Earth. In reality, the Earth is flattened, with the polar radius being about 0.3% smaller than the equatorial radius. If the Earth's oblateness is taken into account, the boundaries of the shadow regions are altered.

Received 23 April 2003; revision received 24 July 2003; accepted for publication 11 September 2003.

*Research Student, Department of Geomatic Engineering; sima@ge.ucl.ac.uk. Member AIAA.

†Research Student, Department of Geomatic Engineering; ants@ge.ucl.ac.uk.

‡Lecturer, Department of Geomatic Engineering.

§Leica Professor of Geomatic Engineering, Department of Geomatic Engineering.

To model accurately the forces acting on the satellite due to solar radiation, it is important to know exactly when the satellite enters or exits a shadow region because the amount of solar radiation incident on the spacecraft drops dramatically. Examples of forces so affected include solar radiation pressure and the recoil force induced by thermal reradiation.

It is perhaps surprising, then, that literature on this topic is so sparse and that the existing material ranges between two extremes. Several techniques use a spherical Earth model because this allows simple geometric arguments to be developed.[1–4] However, it is certainly worthwhile treating the Earth as an oblate spheroid because it has been shown that, with respect to a spherical Earth, the main changes occur in the timing of the umbra and penumbra transitions and in the overall duration of the eclipse periods.[5] Such mistiming has important consequences for the precise numerical integration of orbit trajectories.[6] The main drawback of implementing such a model is that existing approaches for eclipse boundary determination with a spheroidal Earth are significantly more complex than for a spherical Earth. As a result, existing models using a spheroidal Earth are costly to implement in operational software because they are computationally intensive, requiring the use of either a series of rotations[5] or the solution of a quartic equation.[3]

As part of the force modeling work undertaken at University College London by its Geodesy Research Group, a new treatment of the problem has been developed that yields direct solutions for the eclipse state while still accounting for the Earth's polar flattening. This Note presents the mathematical formulation of the method and initial results.

Method to Determine Satellite State

An instantaneous plane is defined by the geocenter, the Earth–sun vector $\boldsymbol{r}_s$ and the Earth–spacecraft vector $\boldsymbol{a}$. In this two-dimensional space, the sun is modeled as a circle. The unit vector orthogonal to the Earth–sun vector is used to find the two required edges of the sun in an Earth centered inertial (ECI) coordinate frame (Fig. 1). The vectors $\boldsymbol{r}_{s1}$ and $\boldsymbol{r}_{s2}$ can be defined as the lines from the geocenter to sun-edge 1 and sun-edge 2, respectively. The method is based on tests that determine whether or not lines from the sun edges to the spacecraft intersect the Earth. If an intersection occurs, and the distance from the sun to this intersection point is less than the sun–spacecraft distance, then the satellite is either in the penumbra or the umbra.

The actual calculations of the intersection points are carried out using three-dimensional geometry, with the surface of the Earth being mathematically approximated by the equation of a spheroid:

$$(x^2 + y^2)/p^2 + z^2/q^2 = 1 \tag{1}$$

where x, y, and z are the ECI coordinates of a point in space on the surface of the spheroid, p is the equatorial radius, and q is the polar radius.

The two lines between the spacecraft and the sun can be defined as follows:

$$(x - a_1)/b_1 = (y - a_2)/b_2 = (z - a_3)/b_3 \tag{2}$$

where a_1, a_2, and a_3 are the x, y, and z components of the position vector of the spacecraft $\boldsymbol{a}$, and b_1, b_2, and b_3 are the x, y, and z components of the vector from either sun-edge 1 or sun-edge 2 to the spacecraft, $\boldsymbol{b}$. Vectors $\boldsymbol{a}$ and $\boldsymbol{b}$ can be obtained for a specific epoch, and hence, the lines are defined. In the plane, rays of light starting at the sun edges and making tangents with the Earth define the full phase/penumbra and penumbra/umbra boundaries, as shown in Fig. 2.

To determine $\hat{\boldsymbol{s}}_p$, the cross product between $\boldsymbol{r}_s$ and $\boldsymbol{a}$ is taken to give a vector $\boldsymbol{r}_i$ normal to the plane:

$$\boldsymbol{r}_i = \boldsymbol{r}_s \times \boldsymbol{a} \tag{3}$$

Taking the cross product of $\boldsymbol{r}_i$ with $\boldsymbol{r}_s$ gives the vector that lies in the plane and is perpendicular to $\boldsymbol{r}_s$, which is $\boldsymbol{s}_p$:

$$\boldsymbol{s}_p = \boldsymbol{r}_s \times \boldsymbol{r}_i \tag{4}$$

Normalizing this vector gives $\hat{\boldsymbol{s}}_p$.